Archives of Biochemistry and Biophysics 512 (2011) 143–153

Contents lists available at ScienceDirect

Archives of Biochemistry and Biophysics

journal homepage: www.elsevier.com/locate/yabbi

Molecular, kinetic, thermodynamic, and structural analyses of *Mycobacterium tuberculosis hisD*-encoded metal-dependent dimeric histidinol dehydrogenase (EC 1.1.1.23)

José E.S. Nunes [a,b], Rodrigo G. Ducati [a], Ardala Breda [a,b], Leonardo A. Rosado [a,b], Bibiana M. de Souza [c], Mario S. Palma [c], Diógenes S. Santos [a,b,*], Luiz A. Basso [a,b,*]

[a] *Centro de Pesquisas em Biologia Molecular e Funcional (CPBMF), Instituto Nacional de Ciência e Tecnologia em Tuberculose (INCT-TB), Pontifícia Universidade Católica do Rio Grande do Sul (PUCRS), Av. Ipiranga 6681, Porto Alegre 90619-900, RS, Brazil*
[b] *Programa de Pós-Graduação em Biologia Celular e Molecular, PUCRS, Porto Alegre, RS, Brazil*
[c] *Instituto de Biociências de Rio Claro, Universidade Estadual Paulista (UNESP), Avenida 24A, 1515, Rio Claro, SP 13506-900, Brazil*

ARTICLE INFO

Article history:
Received 16 March 2011
and in revised form 26 May 2011
Available online 6 June 2011

Keywords:
Histidinol dehydrogenase
Mycobacterium tuberculosis
Metalloenzyme
Thermodynamic binding parameters
Enzyme mechanism
Molecular model

ABSTRACT

The emergence of drug-resistant strains of *Mycobacterium tuberculosis*, the major causative agent of tuberculosis (TB), and the deadly HIV-TB co-infection have led to an urgent need for the development of new anti-TB drugs. The histidine biosynthetic pathway is present in bacteria, archaebacteria, lower eukaryotes and plants, but is absent in mammals. Disruption of the *hisD* gene has been shown to be essential for *M. tuberculosis* survival. Here we present cloning, expression and purification of recombinant *hisD*-encoded histidinol dehydrogenase (*Mt*HisD). N-terminal amino acid sequencing and electrospray ionization mass spectrometry analyses confirmed the identity of homogeneous *Mt*HisD. Analytical gel filtration, metal requirement analysis, steady-state kinetics and isothermal titration calorimetry data showed that homodimeric *Mt*HisD is a metalloprotein that follows a Bi Uni Uni Bi Ping-Pong mechanism. pH-rate profiles and a three-dimensional model of *Mt*HisD allowed proposal of amino acid residues involved in either catalysis or substrate(s) binding.

Introduction

The World Health Organization (WHO) declared tuberculosis (TB)[1] as a global emergency in 1993. Unfortunately, the efforts made by the Stop TB Strategy were not enough to impede the occurrence of 1.3 million deaths in 2009 [1]. However, WHO estimates that the number of cases per capita peaked at 2004 and is slowly falling [2]. Nonetheless, the battle against TB is far from over, since *Mycobacterium tuberculosis* (the main causative agent of TB) proved to be highly adaptive [3] and capable of evading the current strategies for treatment of 0.5 million cases of multi-drug-resistant TB (MDR-TB) that were reported in 2007, including cases of extensively drug-resistant TB (XDR-TB) [2], and the more recently reported totally drug-resistant strains (TDR-TB) [4,5]. To compound the problem further, the deadly association with human immunodeficiency virus makes the treatment of co-infected patients even more challenging [2]. Accordingly, novel TB treatments should, hopefully, reduce the duration of short-course treatment, lower the dose frequency, reduce the pill burden, and present low drug–drug interactions [6].

The histidine biosynthetic pathway has been studied in detail in *Salmonella typhimurium* and *Escherichia coli*. There are 10 enzymatic reactions carried out by eight gene products in the unbranched pathway that include several complex and unusual reactions, and form a critical link between amino acid and purine biosynthesis [7]. The final reaction, first described in *Arthrobacter histidinovorans* and *E. coli* [8], and in yeast [9], is catalyzed by histidinol dehydrogenase (HisD) [L-histidinol:NAD oxidoreductase (EC 1.1.1.23)]. HisD is a bifunctional enzyme that catalyzes the NAD^+- and Zn^{2+}-dependent conversion of L-histidinol (L-Hol) to L-histidine (L-His) through an L-histidinaldehyde (L-Hal) intermediate [8–10], with the concomitant reduction of 2 mol of NAD^+ (Fig. 1A). Previously described HisD enzymes are homodimers [11,12] containing one Zn^{2+} per subunit [11]; and they are

* Corresponding authors at: Av. Ipiranga 6681, Tecnopuc, Prédio 92A, Porto Alegre 90619-900, RS, Brazil. Fax: +55 51 33203629.
E-mail addresses: diogenes@pucrs.br (D.S. Santos), luiz.basso@pucrs.br (L.A. Basso).

[1] *Abbreviations used:* DMSO, dimethyl sulfoxide; DOTS, directly observed treatment short-course; ESI-MS, electrospray ionization mass spectrometry; HisD, histidinol dehydrogenase; IPTG, isopropyl β-D-thiogalactopyranoside; ITC, isothermal titration calorimetry; LB, Luria–Bertani; L-Hol, L-histidinol; L-Hal, L-histidinaldehyde; L-His, L-histidine; MDR, multidrug-resistant; MtHisD, *Mycobacterium tuberculosis* HisD; MWCO, molecular weight cut off; NAD^+, nicotinamide adenine dinucleotide, oxidized form; NADH, nicotinamide adenine dinucleotide, reduced form; PDB, Protein Data Bank; pI, isoelectric point; RMSD, root-mean square deviation; TB, tuberculosis; WHO, World Health Organization; XDR, extensively drug-resistant.

0003-9861 © 2011 Elsevier Inc. Open access under the Elsevier OA license.
doi:10.1016/j.abb.2011.05.020

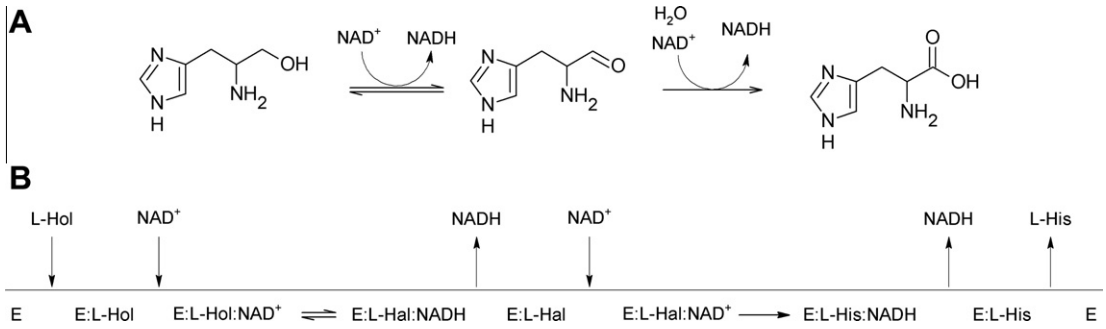

Fig. 1. Chemical reaction catalyzed by HisD. (A) HisD catalyzes the NAD^+- and Zn^{2+}-dependent conversion of L-Hol to L-His through an L-Hal intermediate, with the concomitant reduction of 2 mol of NAD^+. (B) Proposed Bi Uni Uni Bi Ping-Pong enzyme mechanism for *Mt*HisD-catalyzed chemical reaction.

therefore examples of metalloenzymes. Interestingly, it has been pointed out that relatively few other NAD^+-linked oxidoreductases seem to require a bound metal for activity [13].

The histidine biosynthetic pathway is present in bacteria, archaebacteria, lower eukaryotes and plants, but is absent in mammals [14]. Analysis of the complete genome sequence of *M. tuberculosis* H37Rv strain predicted the presence of the coding sequences for the histidine biosynthetic pathway enzymes [15]. The inability of histidine auxotrophs to survive single-amino-acid starvation [16], the identification of genes required for mycobacterial growth [17], and the essentiality of the *hisD* gene product for *M. tuberculosis* survival [18] suggest that HisD is a promising target for antitubercular agent development. Not surprisingly, HisD has been ranked among the top 50 targets by the TDR Targets database [19]. However, it has not been shown yet whether the *hisD* gene codes for a histidinol dehydrogenase activity as predicted by *in silico* analysis of *M. tuberculosis* genome sequence.

The target-based rational design of new agents with anti-TB activity includes functional and structural efforts. However, the first step to enzyme target validation must include experimental data demonstrating that a gene predicted by *in silico* analysis to encode a particular protein catalyzes the proposed chemical reaction. Moreover, recognition of the limitations of high-throughput screening approaches in the discovery of candidate drugs has rekindled interest in rational design methods. Understanding the mode of action of *Mt*HisD should thus inform us on how to better design inhibitors targeting this enzyme with potential therapeutic application in TB chemotherapy.

Here we present cloning, expression, purification to homogeneity, steady-state kinetics, pH-rate profiles, metal requirement studies, isothermal titration calorimetry data on ligand binding, and molecular homology model building of *Mt*HisD. These data prompted the proposal that *Mt*HisD follows a Bi Uni Uni Bi Ping-Pong mechanism. In addition, these studies indicated the likely amino acid residues involved in acid–base catalysis and/or substrate binding. These studies should provide a framework on which to base the rational design of *Mt*HisD enzyme inhibitors to be tested as antiTB agents.

Materials and methods

PCR amplification, cloning and overexpression of recombinant M. tuberculosis hisD-encoded protein

Synthetic oligonucleotide primers (5′-c**cat*atg***cttacccgtatcgacttgcggggag-3′ and 5′-tc**aagctt***gtca*tcgctcgaacctccgccgtac-3′) were designed to be complementary to, respectively, the amino-terminal coding and carboxy-terminal noncoding strands of *hisD* (*Rv1599* locus) gene containing 5′ *Nde*I and 3′ *Hin*dIII restriction sites (in bold), and the start and stop codons (in italics). These primers were used to amplify the *M tuberculosis hisD* structural gene (1317 bp) from genomic DNA using standard PCR conditions (Perkin–Elmer) with a hot start at 99 °C for 10 min. The amplified fragment was purified with CONCERT Nucleic Acid Purification System (Gibco BRL), digested with *Nde*I (Invitrogen) and *Hin*dIII (Gibco BRL), and ligated into a pET-23a(+) expression vector (Novagen). The DNA sequence of the *M. tuberculosis hisD* structural gene was determined using an ABI-PRISM 3100 Genetic Analyzer (Applied Biosystems) to both confirm the identity of the cloned DNA and ensure that no mutations were introduced by the PCR amplification step.

Overexpression was achieved by transforming electrocompetent *E. coli* BL21(DE3) host cells with pET-23a(+)::*hisD* recombinant plasmid and grown on Luria–Bertani (LB) medium containing 50 μg mL^{-1} carbenicillin at 37 °C for 18 h after reaching OD_{600nm} = 0.4 without induction by isopropyl β-D-thiogalactopyranoside (IPTG). Cells were harvested by centrifugation at 12,000*g* for 15 min at 4 °C, and stored at −20 °C.

Protein purification

Approximately 9 g of wet cell paste were suspended in 45 mL of 100 mM Pipes pH 6.0 (buffer A), treated with lysozyme 0.2 mg mL^{-1} at 4 °C for 30 min with gentle stirring, disrupted by sonication with 8 pulses of 15 s each at 60% amplitude with a 13 mm probe. This solution was centrifuged at 48,000*g* for 30 min at 4 °C, and 10 mM $MgCl_2$ (final concentration) and 2000 units of bovine pancreas DNAse I (Sigma) were added to the soluble fraction (~40 U mL^{-1}) under gentle stirring at 4 °C for nucleic acid removal. This mixture was centrifuged at 48,000*g* at 4 °C for 30 min and the supernatant dialyzed against buffer A before being loaded on a Q Sepharose Fast Flow 26/10 (GE Healthcare) column using an Äkta Purifier (GE Healthcare). The column was washed with 4 bed volumes of buffer A and adsorbed protein elution was carried out using a linear gradient of 0–0.5 M NaCl in buffer A. The recombinant *M. tuberculosis* histidinol dehydrogenase (*Mt*HisD) protein eluted at approximately 200 mM NaCl concentration. Fractions were pooled and concentrated using an ultrafiltration membrane with 30 kDa molecular weight cut off (MWCO) and loaded on a HiLoad Superdex 200 26/60 (GE Healthcare) pre-equilibrated with 100 mM Pipes pH 7.2 (buffer B) at 0.8 mL min^{-1}. Fractions containing *Mt*HisD were pooled and loaded on a Mono Q HR 16/10 column (GE Healthcare) equilibrated with buffer B. The column was washed with 2 bed volumes of buffer B and adsorbed protein eluted with a linear 0–0.3 M NaCl gradient in buffer B. Fractions containing homogeneous recombinant *Mt*HisD were dialyzed against buffer B, and stored at −80 °C.

Protein concentration was determined by the method of Bradford [20] using the Bio-Rad protein assay kit (Bio-Rad) and bovine serum albumin as standard.

N-terminal amino acid sequencing and mass spectrometry analysis

Automated Edman degradation was performed with homogeneous *Mt*HisD using a gas-phase sequencer PPSQ-21 A (Shimadzu) to verify N-terminal amino acid sequence. *Mt*HisD was also analyzed by electrospray ionization mass spectrometry (ESI-MS) according to Chassaigne and Lobinski, with some adaptations [21]. The sample was analyzed on Quattro-II triple-quadrupole mass spectrometer (Micromass; Altrincham, UK). During all experiments, the source temperature was maintained at −80 °C and the capillary voltage at 3.6 kV; a drying nitrogen gas flow (200 L h^{-1}) and a nebulizer gas flow (20 L h^{-1}) were used. The mass spectrometer was calibrated with intact horse heart myoglobin and its typical cone voltage-induced fragments. About 50 pmol (10 μl) of each sample was injected into the electrospray transport solvent. The ESI spectrum was obtained in the multichannel acquisition mode, with scanning from 500 to 1800 m/z at a scan time of 7 s. The mass spectrometer is equipped with MassLynx and Transform software for data acquisition and spectrum handling.

Determination of molecular mass and oligomeric state of MtHisD in solution

Analytical gel filtration was performed using a Superdex 200 HR 10/30 (GE Healthcare) column pre-equilibrated with 50 mM Tris HCl pH 7.5 containing 200 mM NaCl at a flow rate of 0.4 mL min^{-1}, with UV detection at 215, 254 and 280 nm. Homogeneous recombinant *Mt*HisD was previously dialyzed against the same buffer. The LMW and HMW Gel Filtration Calibration Kits (GE Healthcare) were used to prepare a calibration curve. The elution volumes (V_e) of standard proteins (ferritin, catalase, aldolase, coalbumin, ovalbumin, ribonuclease A) were used to calculate their corresponding partition coefficient (K_{av}, Eq. (1)). Blue dextran 2000 (GE Healthcare) was used to determine the void volume (V_o). V_t is the total bead volume of the column. The K_{av} value for each protein was plotted against their corresponding molecular mass.

$$K_{av} = \frac{V_e - V_o}{V_t - V_o} \quad (1)$$

Histidinol dehydrogenase assay

HisD catalyzes the sequential NAD^+-dependent oxidations of L-Hol to L-Hal and then to L-His. The enzymatic activity was assayed in the forward direction at 25 °C by continuously monitoring the increase in absorbance at 340 nm due to the conversion of NAD^+ to NADH ($\varepsilon_{NADH} = 6.22 \times 10^3\ M^{-1}\ cm^{-1}$) [22]. One unit of enzyme activity (U) is defined as the amount of enzyme catalyzing the conversion of 1 μmol of substrate per minute. Enzyme inactivation, divalent metal ion activation and determination of steady-state kinetic constants were carried out in 50 mM Pipes pH 7.2. The curves were plotted and steady-state parameters were determined using the nonlinear regression function of Sigma Plot 9.0.

Inactivation by chelating agents

Histidinol dehydrogenases from other organisms have been described as Zn^{2+} metalloenzymes [12,13,23]. In order to investigate whether *Mt*HisD belongs to this class, measurements of enzyme activity were carried out in the presence of 0.1, 1 and 10 mM EDTA and 1, 2 and 5 mM 1,10-phenantroline. All buffers were rendered metal free by treatment with Chelex resin (Bio-Rad).

Divalent metal ion activation

To assess the ability of different divalent metal ions to activate *Mt*HisD enzyme activity, homogeneous enzyme was inactivated with 5 mM 1,10-phenantroline for 5 min and then diluted 10-fold as described by Charles Grubmeyer [13]. After dilution, 10 μL samples were assayed in the presence of Ca^{2+}, Cd^{2+}, Co^{2+}, Mg^{2+}, Mn^{2+}, Ni^{2+} and Zn^{2+}.

Inductively coupled plasma atomic emission spectroscopy (ICP-AES) analysis of metal content

A semi-quantitative analysis was performed to investigate the divalent metals present in the protein sample. A quantitative analysis of Mn^{2+} and Zn^{2+} concentrations in *Mt*HisD homogeneous protein solution was carried out by ICP-AES (Spectro Ciros CCD). Recombinant homogeneous *Mt*HisD was extensively dialyzed against Pipes 100 mM pH 7.2 and concentrated by ultrafiltration to a final protein concentration of 8 mg mL^{-1} (enzyme subunit concentration = 8 mg mL^{-1}/45378.2 Da = 176.3 μM).

Determination of steady-state kinetic parameters and enzyme mechanism

To determine the true steady-state kinetic constants and initial velocity patterns, *Mt*HisD activity was measured in the presence of variable concentrations of L-Hol (10–250 μM) and several fixed-varied concentrations of β-NAD^+ (1–25 mM). Steady-state parameters were calculated by fitting the initial velocity data to Eq. (2) [24]. This equation describes the velocity equation in the absence of products for a Bi Uni Uni Bi Ping Pong Ter Ter System assuming that [B] = [C] and $K_B = K_C$, in which v is the initial velocity, V_{max} is the maximal initial velocity, A and B are the concentrations of the substrates (L-Hol and β-NAD^+), K_A and K_B are their respective Michaelis constants, and K_{iA} is the dissociation constant for enzyme-substrate A (*Mt*HisD:L-Hol) binary complex formation.

$$V = \frac{V_{max}[A][B]}{K_{i,A}K_B + 2K_B[A] + K_A[B] + [A][B]} \quad (2)$$

Isothermal titration calorimetry (ITC) measurements of ligand binding

Isothermal titration calorimetry (ITC) using an iTC_{200} microcalorimeter (Microcal, Inc., Northampton, MA) was performed to assess the enzyme interaction with its substrates and products. ITC measurements were carried out at 25 °C, and titrations were performed using a 39 μL-syringe, with stirring at 500 rpm. Each titration consisted of a preliminary injection of 0.5 μL, followed by 10 injections of 3.85 μL and 180 s intervals between injections, into a cell containing 200 μL of protein sample at 69 μM for substrates and 131 μM for products. Ligand concentrations were 400 μM (L-Hol), 800 μM (L-His) and 50 mM (NAD^+ or NADH). To account for dilution and mixing effects, control experiments were performed injecting ligand into buffer instead of protein in the cell. The control data were subtracted to obtain accurate values for heat changes. The Gibbs free energy (ΔG) of binding was calculated using the relationship described in Eq. (3), in which R is the gas constant (8.314 J K^{-1} mol^{-1}), T is the temperature in Kelvin (T = °C + 273.15), and K_a is the association constant at equilibrium. The entropy of binding (ΔS) can also be determined from this mathematical formula. One set of sites model was utilized to determine the binding and thermodynamic constants. Estimates for K_a and the binding enthalpy (ΔH) were refined by standard Marquardt nonlinear regression method provided in the Origin 7 SR4 software.

$$\Delta G^o = -RT \ln K_a = \Delta H^o - T\Delta S^o \quad (3)$$

pH-rate profiles

To assess the role of acid/base chemistry in the *Mt*HisD enzymatic reaction, apparent steady-state kinetic constants were determined in a composite buffer (100 mM Mes/Hepes/Ches) with pH values ranging from 7.5 to 11.0. The catalytic constants (k_{cat}) and the specificity constants (k_{cat}/K_M) for each substrate were plotted in the logarithm form against pH. The pH-rate profiles were fitted to either Eq. (4) or Eq. (5) [25], in which y is the kinetic parameter (k_{cat} or k_{cat}/K_M), C is the pH-independent value of y, 10^{-pH} is the proton concentration, and K_a and K_b are, respectively, the apparent acid and base dissociation constants for ionizing groups.

$$\log y = \log\left(\frac{C}{1+\frac{10^{-pH}}{K_a}}\right) \quad (4)$$

$$\log y = \left(\frac{C}{1+\frac{K_b}{K_a}+\frac{10^{-pH}}{K_a}+\frac{K_b}{10^{-pH}}}\right) \quad (5)$$

Data described in Fig. 5A and B were best fitted to Eq. (4), which describes a pH-rate profile for a group that needs to be unprotonated (slope of +1) for catalysis (k_{cat}) or L-Hol substrate binding (k_{cat}/K_M). Data given in Fig. 5C were best fitted to Eq. (5), which describes a bell-shaped pH-rate profile for a single ionizing group in the acidic limb that must be unprotonated (slope of +1) for NAD^+ binding and participation of a single ionizing group in the basic limb that must be protonated for substrate binding (slope of −1). It should be pointed out that Eq. (5) describes a bell-shaped pH-rate profile in which the two p*K*s are less than a pH unit apart [25].

Molecular homology model building

The search for templates for the *Mt*HisD target sequence was performed with Blastp [26]. The structure of the homologous *E. coli* protein was selected from the Protein Data Bank (PDB) [27], which was solved experimentally by X-ray diffraction at 1.7 Å resolution (PDB ID: 1KAE). Target and template sequence alignment was performed with ClustalW [28] and required small gaps in both *M. tuberculosis* and *E. coli* HisD amino acid sequences (insertions and/or deletions).

*Mt*HisD protein models were built with restrained-based modeling implemented in MODELLER9v1 [29], with the standard protocol of the comparative protein structure modeling methodology, by satisfaction of spatial restrains [30,31]. The best models were selected according to MODELLER objective function [32] and were subject to energy minimization and stereochemical analysis with PROCHECK [33]. Each subunit of *Mt*HisD homodimer was modeled independently based on the *E. coli* structure, in which subunit A is in the apo form and subunit B has both substrates, histidinol and NAD^+, bound to its active site. Atomic coordinates of heteroatom Zn^{2+} present in both subunits were copied from the template structure into the *Mt*HisD model. Prior to energy minimization, the homodimeric structure was assembled based on the template structure with LEaP module of AMBER7 package [34].

Energy minimization

Energy minimization of the best models were performed with GROMACS package [35] using the 43a1 force-field. The system was submitted to an initial steepest descent energy minimization *in vacuo* with a maximum number of 400 minimization steps, followed by a maximum of 3000 steps of conjugate gradient energy minimization. Identities between the final minimized model of *Mt*HisD and the template were evaluated by their root-mean square deviation (RMSD). Figures were prepared with the PyMOL v0.98 graphics package [36].

Results and discussion

Amplification, cloning, expression and purification of recombinant M. tuberculosis histidinol dehydrogenase (MtHisD)

The probable *hisD* structural gene was PCR amplified from *M. tuberculosis* H37Rv genomic DNA. The presence of 10% DMSO in the reaction mixture proved to be necessary to obtain a PCR product (data not shown). The DMSO cosolvent helps overcome polymerase extension difficulties due to DNA secondary structures and improves the denaturation of GC-rich DNAs [37], which is consistent with the 65.6% G + C content of *M. tuberculosis* genome [15].

The PCR product was cloned into pET-23a(+) expression vector between *Nde*I and *Hin*dIII restriction sites. Nucleotide sequence analysis of the cloned DNA fragment confirmed the identity of the insert as *M. tuberculosis hisD* coding sequence (1317 bp) and demonstrated that no mutations were introduced by the PCR amplification step.

Histidinol dehydrogenase from *M. tuberculosis* H37Rv (*Mt*HisD) was overexpressed in *E. coli* BL21(DE3) electrocompetent host cells transformed with pET-23a(+)::*hisD* recombinant plasmid. To evaluate recombinant *Mt*HisD expression as a function of time, cell growth was tested for 3, 6, 12, 18, 24, and 48 h at 37 °C either with or without IPTG induction. SDS–PAGE analysis revealed a higher yield of soluble recombinant protein in the absence of IPTG for cells grown for 18 h (data not shown). Interestingly, the recombinant *Mt*HisD protein overexpression was achieved with no addition of the inducer. The pET system makes use of a highly processive T7 RNA polymerase under control of the IPTG-inducible *lac*UV5 promoter for the transcription of target genes of interest [38]. Reports have demonstrated that high levels of protein production can be obtained in the stationary phase of cell growth in the absence of IPTG induction [39–41]. It has been proposed that leaky protein expression occurs for *lac*-controlled systems when cells approach stationary phase in complex medium and that cyclic AMP, acetate and low pH are required to affect expression in the absence of IPTG induction [42]. However, it has later been shown that unintended induction in the pET system is likely due to the presence of as little as 0.0001% of lactose in the medium [43].

Purification of recombinant *Mt*HisD has proved to be, at least in our hands, not a trivial task. A number of protocols were attempted to purify *Mt*HisD enzyme to homogeneity with no success, even using a His-tagged construction (data not shown). Incidentally, His-tag purification is not suitable in this case because imidazole, used to elute proteins from affinity columns seems, not surprisingly, to inhibit the enzyme activity. In addition, *Mt*HisD is a metal-dependent enzyme (as will be described in the next section) and the fusion of a His-tag to the recombinant protein could confound interpretation of results. Accordingly, we have opted to use a construction without any fused partner. As *Mt*HisD has a low theoretical isoelectric point (pI = 4.85), it was deemed advantageous to use a pH value as low as possible to reduce the likelihood of *E. coli* proteins being adsorbed to the anion exchange columns (Q Sepharose Fast Flow and Mono Q). Moreover, different substances have different degrees of interaction with the ion exchanger due to differences in their charges, charge densities and distribution of charge on their surfaces, and these interactions can be controlled by varying conditions such as pH. Hence, *Mt*HisD purification protocol employed 100 mM Pipes pH 6.0 buffer for the first Q Sepharose Fast Flow anion exchange column, which resulted in improved recombinant protein yield. Buffer exchange (from buffer A to B) and salt removal were achieved in HiLoad Superdex

Table 1
Typical purification protocol starting from 9 g of cells.

Sample	Total protein (mg)	Total enzyme activity (U)	Specific activity (U mg^{-1})	Purification fold	Yield (%)
Crude extract	693	24	0.03	1.0	100
Q Sepharose	60	28	0.5	17	117
Superdex 200	24	22	0.9	30	92
Mono Q	7.6	10	1.2	40	42

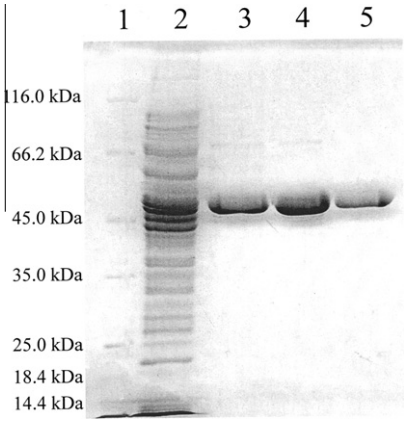

Fig. 2. SDS–PAGE analysis of pooled fractions of desorbed proteins for each purification step. (Lane 1) MW markers (Protein Marker – Fermentas); (Lane 2) crude extract; (Lane 3) Q Sepharose Fast Flow ion exchange; (Lane 4) Superdex 200 gel filtration and (Lane 5) Mono Q ion exchange.

gel filtration column. The third step of the purification protocol employed Mono Q anion exchange column that yielded *Mt*HisD in homogeneous form. This *Mt*HisD purification protocol yielded approximately 7.6 mg of homogeneous enzyme having a specific activity value of 1.2 U mg^{-1} with approximately 40-fold purification using three chromatographic steps (Table 1). SDS–PAGE analysis of total protein content for each chromatographic step is shown in Fig. 2.

N-terminal amino acid sequencing, electrospray ionization mass spectrometry (ESI-MS) analysis, and oligomeric state determination

The first 22 N-terminal amino acid residues were identified as MLTRIDLRGAELTAAELRAALP by Edman degradation sequencing method, in agreement to the *Rv1599* protein-encoded sequence available in the TubercuList database (http://www.genolist.pasteur.fr/TubercuList/). This result unambiguously identifies the purified protein as *Mt*HisD, since the first 22 N-terminal amino acids of HisD from *E. coli* are MSFNTIIDWNSCTAEQQRQLLM.

A value of 45,348.17 Da for the subunit molecular mass of recombinant *Mt*HisD was determined by ESI-MS, which is in reasonably good agreement with the theoretical mass value of 45,378.2 Da. The ESI-MS result also revealed no peak at the expected mass of *E. coli* HisD (46,110.3 Da), thus providing support for the identity of purified recombinant protein. The Edman degradation and ESI-MS results are also consistent with no post-translational removal of N-terminal methionine residue (131.2 Da).

A value of 101.8 kDa for the molecular mass of homogeneous recombinant *Mt*HisD was estimated by gel filtration chromatography (data not shown). This result demonstrates that *Mt*HisD is a dimer in solution, in agreement with HisD enzymes from other organisms [22,23,44].

Table 2
Effect of chelating agents and divalent metal ions on *Mt*HisD enzyme activity.

Chelating agent/metal	(mM)	Specific activity (U mg^{-1})	Percentage (%)
Control		1.47	100
EDTA	0.1	1.74	118
	1	1.98	135
	10	1.41	96
1,10-Phenantroline			
	1	0.68	46
	2	0.38	26
	5	0.05	4
Zn^{2+}	40[a]	0.74	50
Mn^{2+}	40[a]	1.90	129
Mg^{2+}	40[a]	1.07	73
Ca^{2+}	40[a]	0.97	66

[a] Enzyme treated with 5 mM 1,10-phenantroline and diluted 10-fold prior to assay.

Histidinol dehydrogenase as a metalloenzyme

As an attempt to ascertain whether or not *Mt*HisD is a metalloenzyme, EDTA was added to the reaction mixture to observe whether or not there would be a reduction in enzyme activity due to divalent metal capture by the chelating agent. We have previously observed that addition of 0.1 mM of EDTA to *M. tuberculosis* dehydroquinate synthase in the absence of substrates was capable of abolishing enzyme activity after 10 min of incubation [45]. However, direct addition of up to 1 mM EDTA showed no decrease in *Mt*HisD enzyme activity and, even after incubating the enzyme with 10 mM EDTA for 40 min, no loss of enzyme activity could be observed (Table 2). Similar results have been observed for HisD from *S. typhimurium* [13], from which metal content removal was achieved using 1,10-phenantroline. Accordingly, 1 mM 1,10-phenantroline was added to the reaction mixture resulting in a reduction of 46% in *Mt*HisD enzyme activity in comparison to control (Table 2). However, measurements of time-dependent inactivation of enzyme activity demonstrated that there is a need to pre-incubate *Mt*HisD in the presence of 1 mM 1,10-phenantroline for approximately 30 min to completely inactivate the enzyme. Pre-incubation of *Mt*HisD with 5 mM 1,10-phenantroline for 3 min resulted in complete loss of enzyme activity. These results suggest that *Mt*HisD may contain a tightly bound metal that plays an important role in the catalytic activity, which could not be sequestered by EDTA but could be removed by 1,10-phenantroline.

To evaluate divalent metal ions that could possibly rescue *Mt*HisD activity, recombinant enzyme was pre-incubated with 5 mM 1,10-phenantroline for 5 min and diluted 10-fold before measuring enzyme activity. Interestingly, even upon dilution and in the absence of any metal, very low enzyme activity was observed for *Mt*HisD treated with 1,10-phenantroline (data not shown). Addition of Ca^{2+}, Mg^{2+}, Mn^{2+} and Zn^{2+} (40 mM) resulted in regain of *Mt*HisD activity (Table 2), whereas no enzyme activity could be rescued upon addition of Cd^{2+}, Co^{2+} and Ni^{2+} (40 mM) (data not shown), as has been reported for *S. thyphimurium* [13] and cabbage [46] enzymes.

Preliminary analysis to assess metal ion content indicated only the presence of Zn^{2+}, in concentrations above 500 ppm. Metal concentration analysis by ICP-AES yielded the following results: Zn^{2+}, 6.52 mg L^{-1} (99.6 μM) and Mn^{2+}, <0.001 mg L^{-1}. These results suggest a 0.56 ratio (99.6 μM/176.3 μM) of zinc per subunit. These results are in agreement with previously reported data for *S. typhimurium* [13] and *B. oleracea* [47] enzymes. However, the ICP-AES data are somewhat puzzling as 40 mM Mn^{2+} could rescue *Mt*HisD enzyme activity more efficiently than 40 mM Zn^{2+}

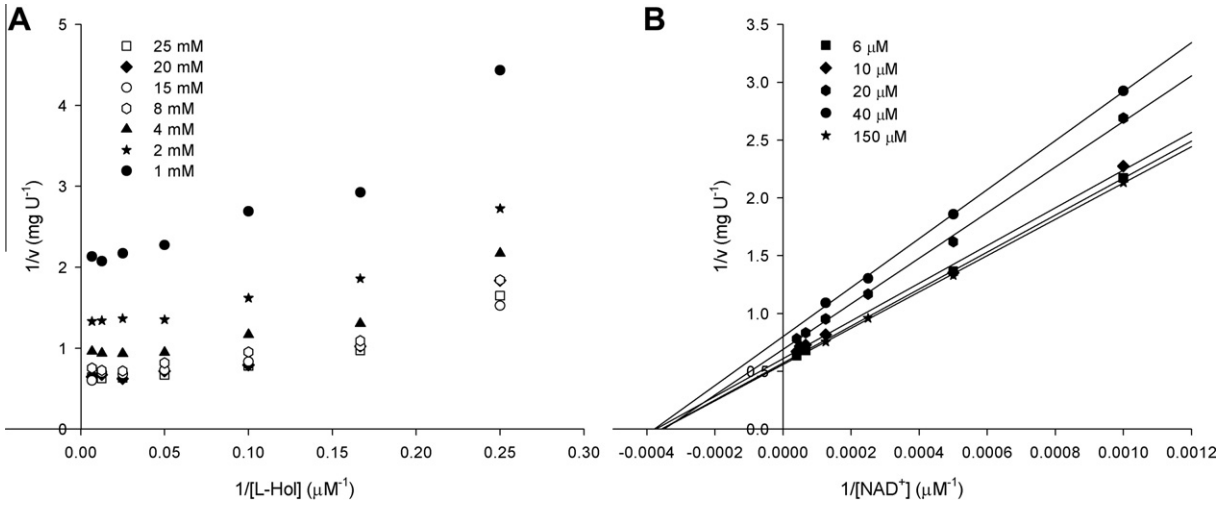

Fig. 3. Double-reciprocal plots of initial velocity experiments. (A) Varying L-Hol concentration a fixed-varied concentrations of NAD^+. (B) Varying and NAD^+, concentration at fixed-varied concentrations of L-Hol. Fixed-varied concentrations of substrates are shown in each graph.

(Table 2). It thus appears not to be warranted to affirm that *Mt*HisD is a Zn^{2+}-dependent enzyme. HisD isolated from spring cabbage heads was shown to be Mn^{2+}-dependent [46]. How to reconcile these apparently contradictory results? A possible explanation is that *Mt*HisD (here reported) was produced as a recombinant protein in *E. coli*, and hence being restricted to the metal content of the host or growth media. The *E. coli* system to import manganese is weakly expressed [48], thereby keeping low intracellular levels of this metal, which could explain why we were unable to demonstrate the presence of Mn^{2+} associated to *Mt*HisD enzyme. It has been demonstrated that Mn^{2+} can promptly replace Zn^{2+} in *S. thyphimurium* HisD enzyme [13]. However, it has been pointed out that the physiological functions of Mn^{2+} in *M. tuberculosis* are still poorly understood, and that several enzyme systems may prove to be Mn^{2+}-dependent however [49].

Steady state kinetics, ITC and enzyme mechanism

The overall reaction catalyzed by HisD can be analyzed as a ter-reactant system in which NAD^+ binds twice to the enzyme during the course of the reaction, and participation of water is ignored as its concentration remains constant. Lineweaver–Burk plots showed a parabolic family of lines for varying L-Hol concentrations and fixed-varied NAD^+ concentrations (Fig. 3A), and a linear pattern of lines was observed for varying NAD^+ concentrations at fixed-varied L-Hol concentrations (Fig. 3B). The double-reciprocal plots for sequential mechanisms that involve *Mt*HisD:L-Hol:2NAD^+ quaternary complex formation would display a non-linear dependence on NAD^+ concentration, including Ordered Ter Ter, partially Random Ter Ter and the completely Random Ter Ter mechanisms [50]. On the other hand, for random mechanisms under steady-state conditions the double-reciprocal plot would show a non-linear dependence on the concentration of L-Hol, even though it binds only once during the reaction sequence [50]. The linear intersecting lines observed for 1/[NAD^+] and the parabolic family of lines for 1/[LHol] may also suggest that *Mt*HisD follows a Ping-Pong mechanism [24]. There are three possible Ping-Pong mechanisms: Bi Uni Uni Bi, Bi Bi Uni Uni, and Hexa Uni [50]. The latter may be discarded as it would give a pattern of parallel lines in double-reciprocal plots for both substrates. A Bi Bi Uni Uni Ping-Pong mechanism would imply that the enzyme would have to exist as a complex with NADH [50]. The value of 45,348.17 Da for the subunit molecular mass of recombinant *Mt*HisD determined by ESI-MS is consistent with the absence of NADH tightly bound to the enzyme as this value should be approximately 46,043.6 Da (45378.2 + 665.4). Accordingly, the initial velocity data were best fitted to Eq. (2) for a Bi Uni Uni Bi Ping-Pong mechanism, yielding values of 1.45 (±0.04)L s^{-1} for k_{cat}, 4.9 (±0.6) × 10^{-6} M for K_M of L-Hol, and 1.4 (±0.1) × 10^{-3} M for K_M of NAD^+.

However, steady-state kinetic data alone could not rule out the random mechanism. Of course, no mechanism is ever proved solely by steady-state kinetic data; at best one can say that given the current data the likely mechanism for *Mt*HisD may be either random or double displacement (Bi Uni Uni Bi Ping-Pong). Equilibrium binary complex formation studies were thus assessed by ITC measurements to both provide thermodynamic signatures of non-covalent interactions to each substrate(s)/product(s) binding processes and distinguish between the possible enzyme mechanisms. No binding of NAD^+ or NADH to free *Mt*HisD enzyme could be detected by ITC measurements (Fig. 4). On the other hand, ITC measurements showed binding of L-Hol and L-His to free *Mt*HisD enzyme (Fig. 4). These results support a Bi Uni Uni Bi Ping-Pong mechanism in which L-Hol substrate binds to free enzyme followed by NAD^+ to form a *Mt*HisD:L-Hol:NAD^+ ternary complex that converts L-Hol into L-Hal and release of NADH from the *Mt*HisD:L-Hal:NADH ternary complex (Fig. 1B). A second NAD^+ molecule binds to *Mt*HisD:L-Hal binary complex to form *Mt*HisD:L-Hal:NAD^+ that converts L-Hal into L-His in the presence of a water molecule followed by release of NADH from *Mt*HisD:L-His:NADH ternary complex yielding the *Mt*HisD:L-His binary complex, from which L-His dissociates to give free *Mt*HisD enzyme for the next round of catalysis (Fig. 1B). It should be pointed out that although the heat flux did not allow reliable estimates for the thermodynamic constants of *Mt*HisD:L-His binary complex formation, it was possible to observe small heat changes between the binding reaction and the control measurement. These data may indicate a large value for the overall dissociation constant for *Mt*HisD:L-His binary complex formation. In any case, the formation of the *Mt*HisD:L-Hol binary complex showed heat changes upon ligand titration (Fig. 4). Fitting the data to one set of sites model yielded the following values for thermodynamic signature of non-covalent interactions upon binary complex formation: net unfavorable enthalpy (ΔH = 3.6 ± 0.5 kcal/mol), favorable entropy (ΔS = 35 ± 13 cal/mol K), and favorable Gibbs energy (ΔG = −7 ± 3 kcal/mol). In addition, the value of 9 (±3) μM for the overall dissociation constant at equilibrium of L-Hol binding to *Mt*HisD is in good

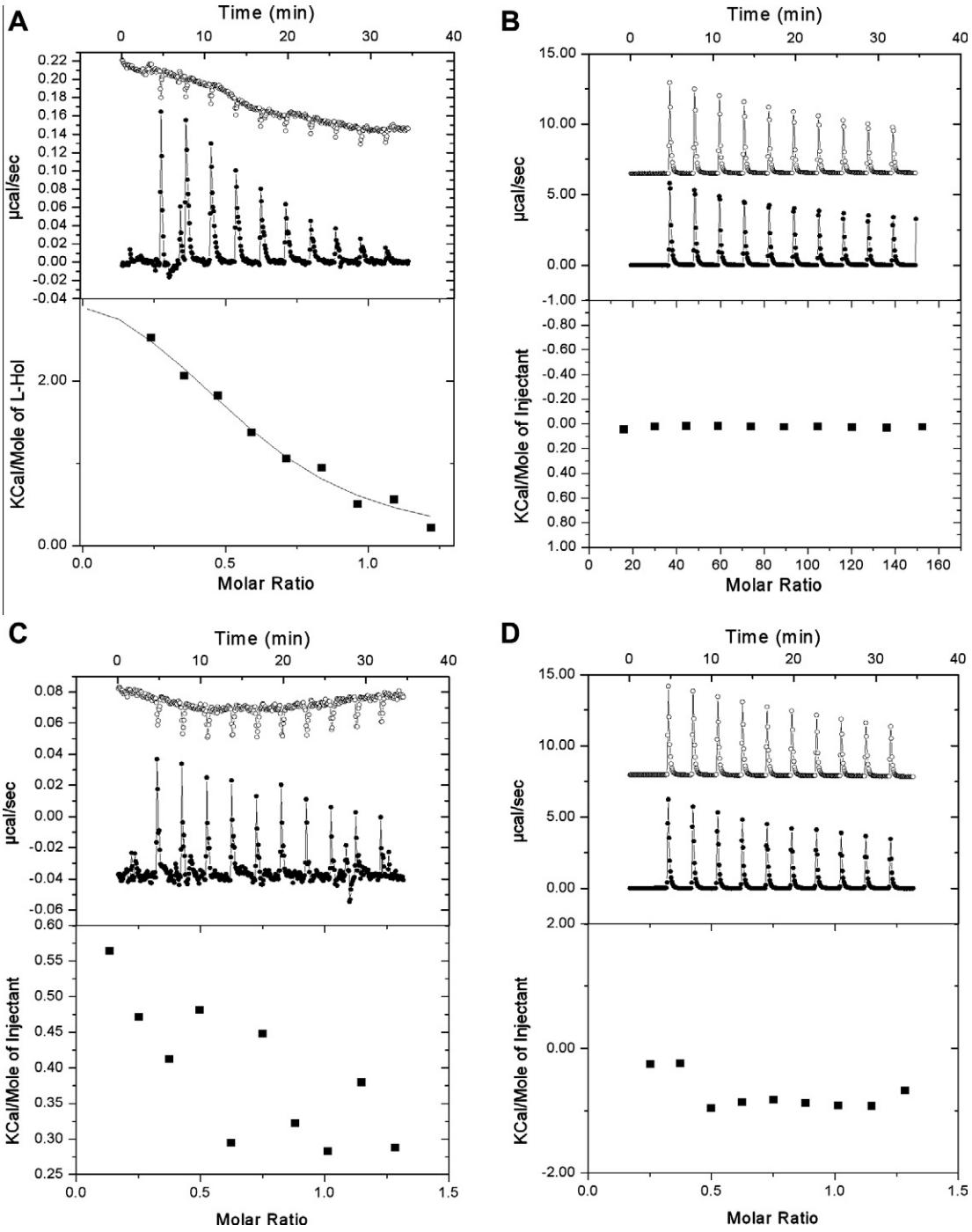

Fig. 4. Isothermal titration calorimetry (ITC) curves for binding of (A) L-Hol (400 µM), (B) NAD^+ (50 mM), (C) L-His (800 µM), and (D) NADH (50 mM) to recombinant *Mt*HisD (69 µM). Control experiments are show as empty circles and titration in the presence of enzyme as filled circles.

agreement with the kinetic data (K_M = 4.9 µM). Interestingly, the unfavorable enthalpy was off-set by the large favorable entropy, resulting in low equilibrium dissociation constant and a spontaneous reaction (ΔG favorable). The observed positive (unfavorable) enthalpy value for *Mt*HisD:L-Hol formation may be due to an unfavorable redistribution of the network of interatomic interactions (e.g., hydrogen bonds and van der Walls) between the reacting species (including solvent) [51]. The observed positive (favorable) entropy value for L-Hol binding to free *Mt*HisD may be associated with release of "bound" water molecules from the surface to the bulk solvent [51].

pH-rate profiles

To probe for acid–base catalysis, pH dependence studies of k_{cat}, and k_{cat}/K_M for L-Hol and NAD^+ were performed. The pH-rate data for k_{cat} were fitted to Eq. (4), indicating that protonation of a group (slope of +1) with an apparent p*K* value of approximately 8 (±1) (Fig. 5) abolishes catalysis. The pH-rate data for k_{cat}/K_M for L-Hol were fitted to Eq. (4), suggesting that protonation of a group (slope of + 1) with an apparent p*K* value of approximately 8 (± 3) is required for binding of L-Hol to free *Mt*HisD (Fig. 5). These pK_a's values may be attributed to conserved histidine residues present

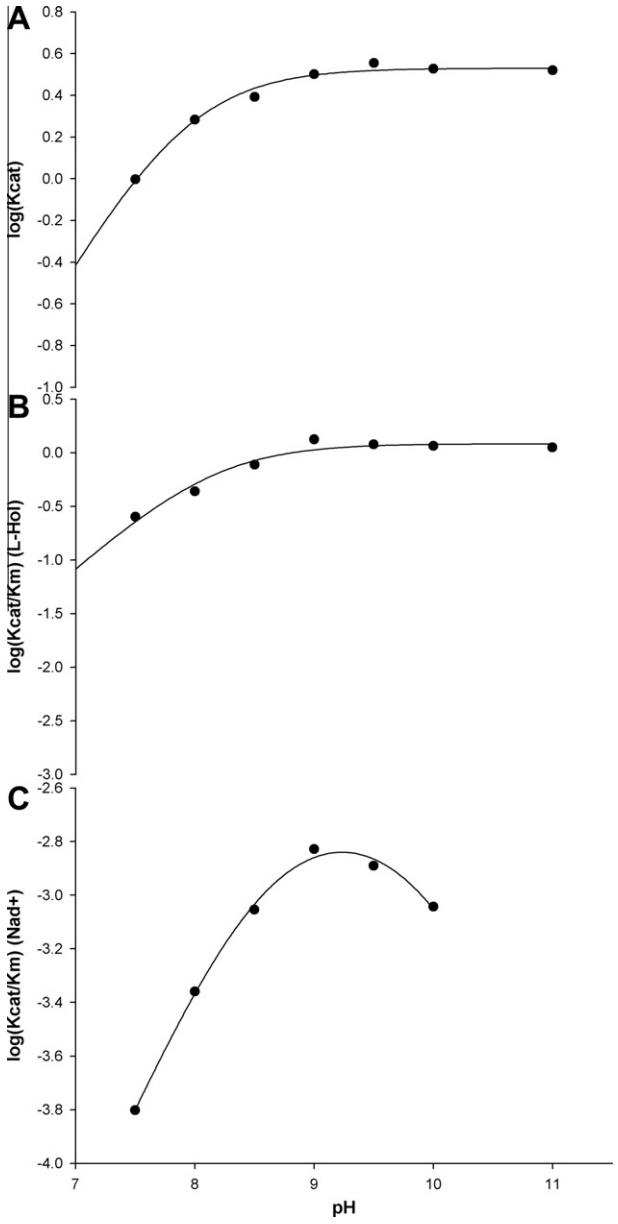

Fig. 5. pH-rate profiles for the reaction catalyzed by *Mt*HisD. Steady-state kinetic constants were plotted in the logarithmic form against the pH value of the assay mixture. (A) pH dependence of log k_{cat} data were fitted to Eq. (4); (B) pH dependence data of k_{cat}/K_M for L-Hol were fitted to Eq. (4); (C) pH dependence data of k_{cat}/K_M for NAD^+ were best fitted to Eq. (5).

in the active site (Fig. 6). Although the observed p*K* values for imidazole side chain of L-His range from 6.0 to 7.0, amino acid residues in biologically active proteins may have very different chemical properties. A number of reports have shown similar pH profiles suggesting that the side chain of histidine residue acts as a base assisting the proton transfers during the overall catalysis [47,52,53]. For instance, a value of log(k_{cat}) and log(k_{cat}/K_M) titration profiles for the overall reaction with L-Hol as the variable substrate indicated that the deprotonated form of a single ionizable group with p*K* of 8.17 and 8.35 was essential for, respectively, catalysis and substrate binding to *S. typhimurium* HisD [52]. Essential roles for histidines in HisD mode of action have also been shown by site-directed mutagenesis [47,53] and structural studies [23]. The crystal structure of *E. coli* HisD [23] showed that the hydroxyl group of L-Hol forms H-bonds to the backbone carbonyl of His367 (corresponding to His376 in *Mt*HisD) and to the $His327^{N\varepsilon 2}$ atom (corresponding to His336 in *Mt*HisD). It is thus tempting to suggest that the conserved imidazole group of His336 plays a critical role in both catalysis and L-Hol binding to *Mt*HisD. The data for k_{cat}/K_M for NAD^+ were best fitted to Eq. (5), which describes a bell-shaped pH-rate profile for a single ionizing group in the acidic limb that must be unprotonated for NAD^+ binding and participation of a single ionizing group in the basic limb that must be protonated for substrate binding. These p*K* values differ by less than a pH unit however. Data fitting yielded an apparent p*K* value of 9.2, which is a mean of the two residues. The *E. coli* HisD structure showed the phosphate groups of NAD^+ make H-bonds to Asn211, Tyr130, and Gly133 via a bridging water molecule [23]. The adenosine sugar O2′ is H-bonded to Gln188 side chain, whereas O4′ interacts with Asn211, and the adenine N3 atom makes an H-bond to Gln188 via a water molecule [23]. The two likely candidates that play a role in NAD^+ binding to *Mt*HisD are the conserved Tyr129 and Tyr223 (Fig. 6). Although the sequence alignment helps infer amino acids involved in catalysis and/or binding, the molecular model (presented in more detail in the next section) suggests that the Tyr129, Tyr223 and His335 residues make contacts with the substrates in the *Mt*HisD enzyme active site (Fig. 7). Notwithstanding, the rate expression for k_{cat}/K_M starts with the combination of substrate and enzyme and includes all steps through the first irreversible one, which is usually either release of the first product or an irreversible chemical step prior to this. In addition, the pH-dependent profile for k_{cat} reports on events following the enzyme-substrate complex formation capable of undergoing catalysis, which include the chemical steps, possible enzyme conformational changes, and product release (leading to regeneration of free enzyme). Hence, the ionization of a group observed in the pH profile for k_{cat}/K_M includes both binding and catalytic steps. Accordingly, participation of ionizing groups solely in catalysis cannot be ruled out for the p*K*s derived from the acidic limbs of the pH profiles for k_{cat}/K_M (Fig. 5B and C). On the other hand, participation of a single ionizing group in the basic limb with apparent p*K* value of 9.2 derived from the pH profile of k_{cat}/K_M for NAD^+ can be attributed to substrate binding, as the pH profile for k_{cat} shows no ionizing group involved in catalysis in the basic limb (Fig. 5C). At any rate, site directed mutagenesis efforts should be pursued to assign a definite role in catalysis and/or binding to these amino acid side residues.

Three-dimensional model analysis

The three-dimensional structure of *E. coli* HisD has been determined by X-ray diffraction in the apo state as well as in complex with L-Hol, Zn^{+2} and NAD^+ at 1.7 Å resolution [23], which was employed as template for molecular homology modeling of *Mt*HisD structure. *E. coli* HisD protein sequence is four amino acids shorter than *Mt*HisD (434 and 438 amino acids, respectively). Although small gaps were included, there exists high sequence conservation with 36% identity (Fig. 6), which satisfies homology modeling premises [30] and lends support to using *E. coli* HisD as a suitable template. There are no major structural rearrangements upon NAD^+, L-Hol, and Zn^{2+} binding as compared to the apo form of *E. coli* HisD [23], with RMSD value of just 1 Å when all alpha carbon coordinates are considered. Stereochemical analysis by PROCHECK [33] showed that 91% of *Mt*HisD amino acid residues are in the most favored regions of the Ramachandran plot, validating our model as suitable for structural inferences.

Most significant structural variations are observed at the C-termini of each *Mt*HisD subunit (RMSD value of 3.08 Å). The HisD monomer consists of four domains; two larger globular domains (domain 1, amino acid residues 25–103, 124–247 and domain 2, amino acids 1–24, 237–381) with an α/β/α topology, in which

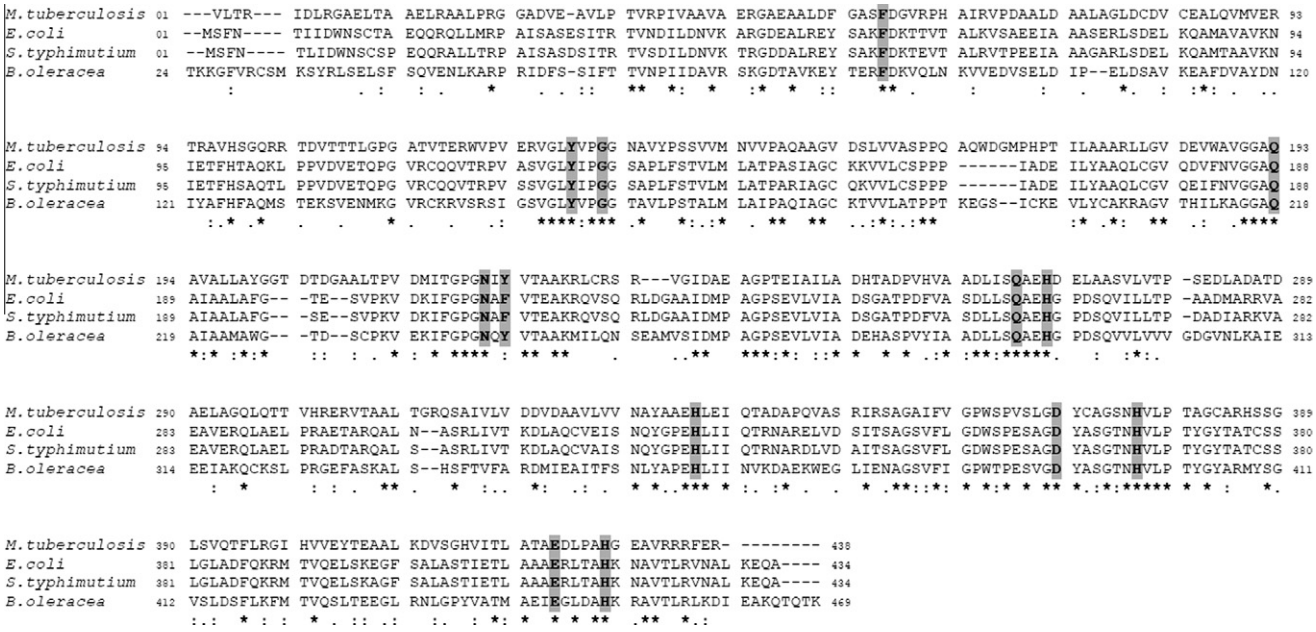

Fig. 6. Neighbor-joining multi sequence alignment of *M. tuberculosis* (TubercuList: Rv1599), *E. coli* (UniProt: P06988), *S. thyphimurium* (GenBank: NP_461017.1) and *B. oleracea* (GenBank: AAA32991.1) HisD enzymes, performed with ClustalW (1). *B. oleracea* first 23 amino acids were omitted from alignment. Amino acid conservation, strong similarity, weak similarity and in/del are denoted as, respectively, ∗, :, ., and –. Amino acids involved in substrates binding are shaded in gray.

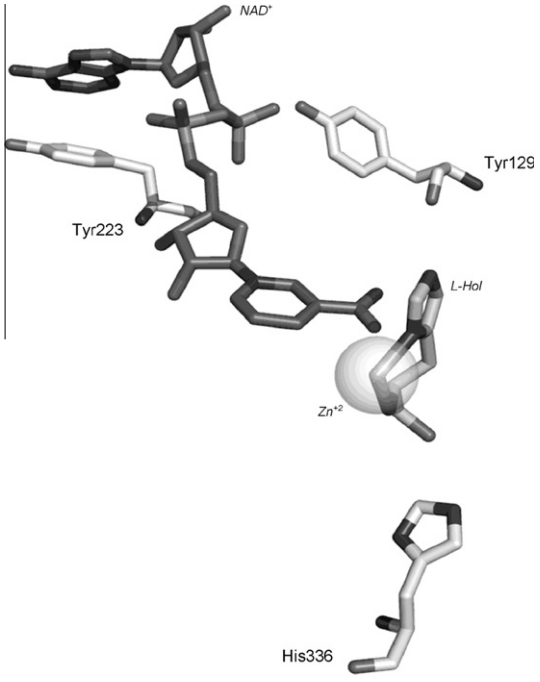

Fig. 7. Proposed *Mt*HisD residues involved in substrate binding and/or catalysis. All residues are less than 4.0 Å from substrates.

the core of both globular domains adopt incomplete Rossmann folds lacking one strand-helix hairpin. A third domain (domain 3, amino acids 104–123 and 400–409) is composed by a three-stranded antiparallel β-sheet that extends away from the two globular domains. The fourth domain (domain 4, residues 410–437) folds into a small V-shaped two-helical hairpin that is perpendicular to the third domain antiparallel β-sheet (Fig. 8A). Structural variation is observed at the C-termini, explicitly at domain 4, where the second helix of the helical hairpin has moved away from the substrate and Zn^{+2} binding site (Fig. 8B). This displacement of ~7 Å of the side chains of the amino acids involved in L-Hol and Zn^{+2} binding may be a result of domain 4 flexibility. The crystallographic structure of *E. coli* HisD showed no major structural rearrangement upon binding of substrates [23].

Substrate and Zn^{+2} binding sites are located on the homodimer interface, NAD^+ binding site is located at domain 1, at the incomplete Rossmann fold structural motif. *Mt*HisD amino acids involved in L-Hol binding are His336 and His376 from domain 2 and Glu423 of domain 4 (Fig. 6). The Zn^{+2} ion is octahedrally coordinated to Gln267, His270, Asp369, His428, and two ligands from L-Hol. Amino acid residues contributing to NAD^+ binding include Tyr129, Gly132, and Asn221 (phosphate binding); Gln193 and Asn221 (adenosine sugar binding); and Phe58, Gln193, and Tyr223 (adenine base binding). The conservation of these amino acid residues is noticeable, being all but Tyr223 conserved among *Mt*HisD homologues (Fig. 6). Although not directly involved in HisD catalysis, Zn^{+2} interacts with the amino group of histidinol that has been suggested to play a role in the correct positioning of L-Hol in the enzyme active site [23].

A proposal for the *E. coli* HisD reaction mechanism has been put forward which involves abstraction of the hydroxyl group proton of L-Hol by His327 (*Mt*HisD His336) and concomitant hydride transfer from the reactive carbon (carbon bound to the hydroxyl group that upon hydride transfer adopts the sp2 configuration) to NAD^+, forming L-Hal and transiently protonated His327 (*Mt*HisD His336) [23]. A neighboring water molecule is activated by Glu326 (*Mt*HisD Glu335) to make a nucleophilic attack on the carbonyl carbon with concomitant protonation of aldehyde oxygen by the transiently protonated His327 (*Mt*HisD His336), leading to the formation of an L-histidindiol (gem-diol) intermediate. Hydride transfer to NAD^+ from now sp3-gem-diol carbon of $-CH-(OH)_2$ intermediate with concomitant proton abstraction from a substrate hydroxyl group by unprotonated His327 (*Mt*HisD His336) form the sp2-carbon of the carboxylate group of L-His. The protonated His327 (*Mt*HisD His336) is thought to donate a proton to a water molecule. NMR studies indicated that the metal ion interacts with the imidazole portion of the substrate and acts as a Lewis acid

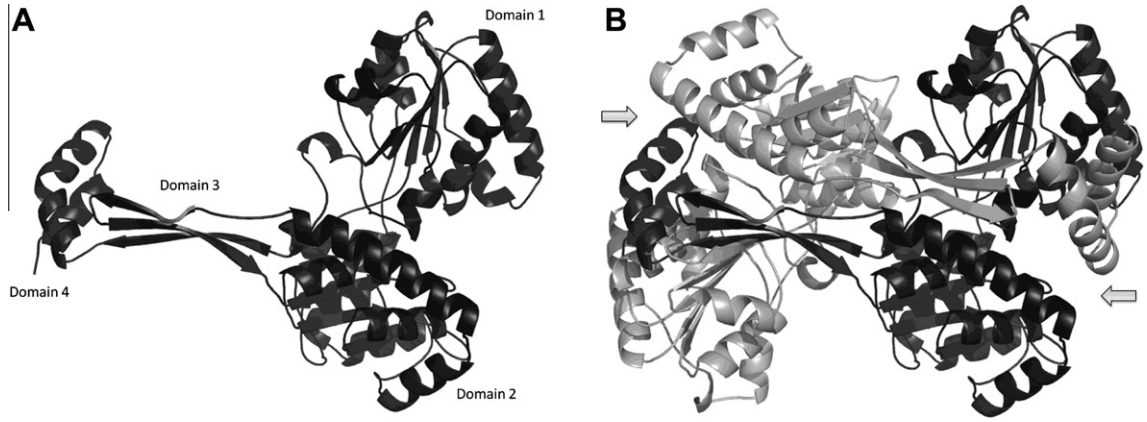

Fig. 8. Molecular model of *Mt*HisD. (A) Three-dimensional structure of the *Mt*HisD monomer, indicating its globular domains (1 and 2), the helical-hairpin (domain 4), and the connective three-stranded antiparallel β-sheet (domain 3). (B) *Mt*HisD homodimeric three-dimensional structure, subunit A in light gray and subunit B in dark gray. The L-shaped arm formed by domains 3 and 4 extends from each monomer and forms a latch-like structure that closes upon domains 1* and 2* of the other monomer (asterisks are residues from the neighboring monomer). The two active sites of *Mt*HisD protein are located at the boundaries of the homodimer interface (arrows). Amino acid residues from both subunits make H- bonds to L-Hol and Zn^{2+} (domains 1, 2, and 4*); and NAD^+ is H-bonded to amino acids from domain 1.

inducing polarization of the carbonyl group to increase the susceptibility to nucleophilic attack for the aldehyde oxidation [54]. However, structural analysis of *E. coli* HisD prompted the authors to suggest that Zn^{2+} plays a role in proper positioning of L-Hol [23]. As pointed out in the previous section, the conserved imidazole group of His336 is likely the residue with p*K* value of approximately 8 that plays a critical role in catalysis and L-Hol binding (Fig. 5A and B). A value ranging from 4.3 to 4.5 is usually observed for p*K* of the γ-carboxyl group of glutamate, although it depends on the chemical context of an enzyme active site. The pH-rate data for *Mt*HisD have not provided a clear evidence for participation of, for instance, Glu335 in either catalysis or substrate binding. Accordingly, site-directed mutagenesis will have to be pursued to reveal whether or not this amino acid side chain plays any role in the mode of action of *Mt*HisD enzyme.

Conclusion

In the present work, PCR amplification, cloning and sequencing of *hisD* gene from *M. tuberculosis* H37Rv strain are described. Data on recombinant *Mt*HisD protein purification, N-terminal amino acid sequencing and electrospray ionization mass spectrometry analyses were presented to confirm the identity of the recombinant protein. Analytical gel filtration, inactivation by chelating agents, activation by divalent metal ions, and inductively coupled plasma atomic emission spectroscopy (ICP-AES) analysis of metal content indicated that *Mt*HisD is a homodimeric metalloprotein. Steady-state kinetics and ITC studies suggested that *Mt*HisD follows a Bi Uni Uni Bi Ping-Pong mechanism, in which L-Hol substrate binds to free enzyme followed by NAD^+ to form a *Mt*HisD:L-Hol:NAD^+ ternary complex that converts L-Hol into L-Hal and release of NADH from the *Mt*HisD:L-Hal:NADH ternary complex. A second NAD^+ molecule binds to *Mt*HisD:L-Hal binary complex to form *Mt*HisD:L-Hal:NAD^+ that converts L-Hal into L-His in the presence of a water molecule followed by release of NADH from *Mt*HisD:LHis:NADH ternary complex yielding the *Mt*HisD:L-His binary complex, from which L-His dissociates to give free *Mt*HisD enzyme for the next round of catalysis. Based on pH-rate profiles, primary sequence comparisons, and molecular homology modeling of *Mt*HisD, the likely amino acid residues involved in acid–base catalysis and/or substrate binding are proposed. Further efforts to provide a more detailed picture of *Mt*HisD mode of action will include, but not be limited to, site-directed mutagenesis, chemical rescue, isotope effects, pre-steady state kinetics, and crystal structure determination.

Acknowledgments

This work was supported by funds of Decit/SCTIE/MS-MCT-CNPq-FNDCT-CAPES to National Institute of Science and Technology on Tuberculosis (INCT-TB) to D.S.S. and L.A.B. L.A.B. and D.S.S. also acknowledge financial support awarded by FAPERGS-CNPq-PRONEX-2009. D.S.S. (CNPq, 304051/1975-06) and L.A.B. (CNPq, 520182/99-5) and are Research Career Awardees of the National Research Council of Brazil (CNPq). J.E.S.N. and L.A.R. acknowledge scholarships awarded by CNPq. A.B. acknowledges a scholarship awarded by BNDES.

References

[1] World Health Organization, Global tuberculosis control: WHO report 2010, Geneva, Switzerland, WHO/HTM/TB/2010.7.
[2] World Health Organization, Global tuberculosis control: epidemiology, strategy, financing, WHO report 2009, Geneva, Switzerland, WHO/HTM/TB/2009.411.
[3] D. Kumar, K.V.S. Rao, Regulation between survival persistence, Microbes Infect. 13 (2011) 121–133.
[4] A.A. Velayati, P. Farnia, M.R. Masjedi, T.A. Ibrahim, P. Tabarsi, R.Z. Haroun, H.O. Kuan, J. Ghanavi, P. Farnia, M. Varahram, Totally drug-resistant tuberculosis strains: evidence of adaptation at the cellular level., Eur. Resp. J. 34 (2009) 1202–1203.
[5] A.A. Velayati, Chest 136 (2009) 420–425.
[6] A. Koul, E. Arnoult, N. Lounis, J. Guillemont, K. Andries, Nature 469 (2011) 483–490.
[7] M.E. Winkler, Biosynthesis of Histidine, in: F.C. Neidhardt (Ed.), *Escherichia coli* and *Salmonella*: Cellular and Molecular Biology, ASM Press, Washington, DC, 1996, pp. 485–505.
[8] E. Adams, J. Biol. Chem. 209 (1954) 829–846.
[9] E. Adams, J. Biol. Chem. 217 (1955) 325–344.
[10] J.C. Loper, E. Adams, J. Biol. Chem. 240 (1965) 788–795.
[11] S.Y. Lee, C.T. Grubmeyer, J. Bacteriol. 169 (1987) 3938–3944.
[12] A. Nagai, K. Suzuki, E. Ward, M. Moyer, M. Hashimoto, J. Mano, D. Ohta, A. Scheidegger, Arch. Biochem. Biophys. 295 (1992) 235–239.
[13] C. Grubmeyer, M. Skiadopoulos, A.E. Senior, Arch. Biochem. Biophys. 272 (1989) 311–317.
[14] D. Voet, J.D. Voet, Amino acid metabolism, in: D. Voet, J.D. Voet (Eds.), Biochemistry, John Wiley & Sons, Inc., USA, 1995, pp. 727–784.
[15] S.T. Cole, R. Brosch, J. Parkhill, T. Garnier, C. Churcher, D. Harris, S.V. Gordon, K. Eiglmeier, S. Gas, C.E. Barry III, F. Tekaia, K. Badcock, D. Basham, D. Brown, T. Chillingworth, R. Connor, R. Davies, K. Devlin, T. Feltwell, S. Gentles, N. Hamlin, S. Holroyd, T. Hornsby, K. Jagels, B.G. Barrel, Nature 393 (1998) 537–544.
[16] T. Parish, J. Bacteriol. 185 (2003) 6702–6706.
[17] C.M. Sassetti, D.H. Boyd, E.J. Rubin, Mol. Microbiol. 48 (2003) 77–84.
[18] T. Parish, B.G. Gordhan, R.A. McAdam, K. Duncan, V. Mizrahi, N.G. Stoker, Microbiology 145 (1999) 3497–3503.

[19] F. Agüero, B. Al-Lazikani, M. Aslett, M. Berriman, F.S. Buckner, R.K. Campbell, S. Carmona, I.M. Carruthers, A.W.E. Chan, F. Chen, G.J. Crowther, M.A. Doyle, C. Hertz-Fowler, A.L. Hopkins, G. McAllister, S. Nwaka, J.P. Overington, A. Pain, G.V. Paolini, U. Pieper, S.A. Ralph, A. Riechers, D.S. Roos, A. Sali, D. Shanmugam, T. Suzuki, W.C. Van Voorhis, C.L.M.J. Verlinde, Nat. Rev. Drug Discov. 7 (2008) 900–907.
[20] M.M. Bradford, Anal. Biochem. 72 (1976) 248–254.
[21] H. Chassaigne, R. Lobinski, Analyst 123 (1998) 2125–2130.
[22] A. Kheirolomoom, J. Mano, A. Nagai, A. Ogawa, G. Iwasaki, D. Ohta, Arch. Biochem. Biophys. 312 (1994) 493–500.
[23] J.A.R.G. Barbosa, J. Sivaraman, Y. Li, R. Larocque, A. Matte, J.D. Schrag, M. Cygler, Proc. Natl. Acad. Sci. USA 99 (2002) 1859–1864.
[24] I.H. Segel, Enzyme Kinetics – Behavior Analysis of Rapid Equilibrium and Steady-state Enzyme Systems, Wiley, Classics Library Edition, Wyley-Interscience Publication, John Wiley & Sons, Inc., New York, 1993.
[25] P.F. Cook, W.W. Cleland, Enzyme Kinetics and Mechanism, Garland Science, New York, 2007.
[26] S.F. Altschul, T.L. Madden, A.A. Schäffer, J. Zhang, Z. Zhang, W. Miller, D.J. Lipman, Nucleic Acids Res. 25 (1997) 3389–3402.
[27] H.M. Berman, J. Westbrook, Z. Feng, G. Gilliland, T.N. Bhat, H. Weissig, I.N. Shindyalov, P.E. Bourne, Nucleic Acids Res. 28 (2000) 235–242.
[28] J.D. Thompson, D.G. Higgins, T.J. Gibson, Nucleic Acids Res. 22 (1994) 4673–4680.
[29] A. Šali, T.L. Blundell, J. Mol. Biol. 234 (1993) 779–815.
[30] M.A. Martí-Renom, A.C. Stuart, A. Fiser, R. Sánchez, F. Melo, A. Šali, Annu. Rev. Biophys. Biomol. Struct. 29 (2000) 291–325.
[31] A. Šali, J.P. Overington, Protein Sci. 3 (1994) 1582–1596.
[32] M.Y. Shen, A. Šali, Protein Sci. 15 (2006) 2507–2524.
[33] R.A. Laskowski, M.W. MacArthur, D.S. Moss, J.M. Thornton, J. Appl. Cryst. 26 (1993) 283–291.
[34] D.A. Case, D.A. Pearlman, J.W. Caldwell, T.E. Cheatham III, J. Wang, W.S. Ross, C.L. Simmerling, T.A. Darden, K.M. Merz, R.V. Stanton, A.L. Cheng, J.J. Vincent, M. Crowley, V. Tsui, H. Gohlke, R.J. Radmer, Y. Duan, J. Pitera, I. Massova, G.L. Seibel, U.C. Singh, P.K. Weiner, P.A. Kollman, AMBER 7. University of California, San Francisco, 2002.
[35] D. van der Spoel, E. Lindahl, B. Hess, G. Groenhof, A.E. Mark, H.J.C. Berendsen, J. Comp. Chem. 26 (2005) 1701–1718.
[36] W.L. DeLano, The PyMOL Molecular Graphics System. DeLano Scientific, San Carlos, CA, USA, 2002, Available from: <http://www.pymol.org>.
[37] P.R. Winship, Nucleic Acids Res. 17 (1989) 1266.
[38] K.C. Kelley, K.J. Huestis, D.A. Austen, C.T. Sanderson, M.A. Donoghue, S.K. Stickel, E.S. Kawasaki, M.S. Osburne, Gene 156 (1995) 33–36.
[39] J.S. Oliveira, C.A. Pinto, L.A. Basso, D.S. Santos, Protein Expr. Purif. 22 (2001) 430–435.
[40] M.L. Magalhaes, C.P. Pereira, L.A. Basso, D.S. Santos, Protein Expr. Purif. 26 (2002) 59–64.
[41] R.G. Silva, L.P. Carvalho, J.S. Oliveira, C.A. Pinto, M.A. Mendes, M.S. Palma, L.A. Basso, D.S. Santos, Protein Expr. Purif. 27 (2003) 158–164.
[42] T.H. Grossman, E.S. Kawasaki, S.R. Punreddy, M.S. Osburne, Gene 209 (1998) 95–103.
[43] F.W. Studier, Protein Expr. Purif. 41 (2005) 207–234.
[44] E. Burger, H. Gorisch, F. Lingens, Biochem. J. 181 (1979) 771–774.
[45] J.D. de Mendonça, O. Adachi, L.A. Rosado, R.G. Ducati, D.S. Santos, L.A. Basso, Mol. BioSyst. 7 (2011) 119–128.
[46] A. Nagai, A. Scheidegger, Arch. Biochem. Biophys. 284 (1991) 127–132.
[47] A. Nagai, D. Ohta, J. Biochem 115 (1994) 22–25.
[48] A. Anjem, S. Varghese, J.A. Imlay, Mol. Microbiol. 72 (2009) 844–858.
[49] D. Agranoff, S. Krishna, Front. Biosci. 9 (2004) 2996–3006.
[50] H. Görisch, Biochem. J. 181 (1979) 153–157.
[51] R. O'Brien, I. Haq, Applications of Biocalorimetry: Binding, Stability and Enzyme Kinetics, in: J.E. Ladbury, M.L. Doyle (Eds.), Biocalorimetry 2: Applications of Calorimetry in the Biological Sciences, John Wiley & Sons, Ltd., West Sussex, 2004, pp.3–34.
[52] C. Grubmeyer, H. Teng, Biochemistry 38 (1999) 7355–7362.
[53] H. Teng, C. Grubmeyer, Biochemistry 38 (1999) 7363–7371.
[54] K. Kanaori, N. Uodome, A. Nagai, D. Ohta, A. Ogawa, G. Iwasaki, A.Y. Nosaka, Biochemistry 35 (1996) 5949–5954.